NANO LETTERS

2007
Vol. 7, No. 3
837−842

Mesoscale Engines by Nonlinear Friction

D. Fleishman,[†] J. Klafter,[†] M. Porto,[‡] and M. Urbakh*,[†]

School of Chemistry, Tel Aviv University, 69978 Tel Aviv, Israel, Institut für Festkörperphysik, Technische Universität Darmstadt, 64289 Darmstadt, Germany

Received January 2, 2007; Revised Manuscript Received February 1, 2007

ABSTRACT

A new approach to build mesoscopic-size engines that move translationally or rotationally and can perform useful functions such as the pulling of a cargo is presented. The approach is based on the transformation of internal vibrations of the moving object into directed motion, making use of the nonlinear properties of friction. This can be achieved by superimposing time-dependent external fields that break the spatial symmetry. The motion can be controlled and optimized by adjusting the system parameters.

Macroscale thermodynamic engines convert random motion due to fuel-produced heat into directed motion. Such engines cannot be downsized to the micro- and nanometer scales because thermodynamics does not apply to single atoms or molecules, but rather to large assemblies. Hence a great challenge for the field of nanotechnology is the design and construction of microscopic motors that can transform input energy into directed or programmed motion and perform useful functions such as transporting cargo.

While a few steps in this direction have already been made experimentally,[1,2] the investigation of how to transform externally supplied energy in an efficient and controllable way into performing specific functions on the molecular scale is still at its early stages. Most studies in this field, which have focused on the so-called Brownian motors, relied on the idea of particles moving in spatially asymmetric ratchet potentials under the influence of stochastic and/or periodic forces.[3−5] Recently, an alternative concept has been proposed[6−8] in which directed motion of molecular-scale engines is achieved dynamically and no static asymmetry, which has to be built into in the system, is required. Essential to this approach is a presence of spatially inhomogeneous (for instance, periodic) interaction between a moving object and an underlying substrate, which is corrugated on the length scale of the engine. Then, achieving motion of the engine is based on dynamical competition between the two intrinsic lengths scale, that of the substrate and the object.

In this paper, we demonstrate that a similar mechanism of transforming fed energy into directed motion can be also realized in the case of spatially uniform substrates. The only necessary condition for this is a nonlinear dependence of the friction between the moving object and the substrate on the relative velocity. These conditions are rather common for mesoscale objects with sizes ranging from tenths of nanonometers to micrometers. At these length scales, typical substrates can be considered as spatially uniform. Motion of a mesoscale-size object on a substrate involves interaction of large ensemble of asperities that give rise to static friction (the force necessary to start sliding) and velocity-dependent kinetic friction (the force necessary to keep sliding at a given velocity).[9] The dynamical response of such systems is nonlinear because the frictional force in a sliding state differs from the static friction.

The ability to produce directed motion at the nanometer to micrometer scales is of broad interest in micromachining applications ranging from optics to memory storage and medical devices.[10] To meet high-precision positioning requirements, these devices should be able to control the elementary step sizes and to allow long-range motion. Here we show that all these requirements can be satisfied within the proposed approach. The velocity of the engine can be varied over a wide range, independent of the direction; the engine is powerful enough to allow for the transportation of a cargo, and the same concept applies for both translational and rotational motions.

Consider the model system which includes three identical blocks each of mass m connected by two identical linear springs of spring constant K. The three blocks are numbered 1, 2, and 3 (from right to left), whereas the two springs are denoted by 1 (right) and 2 (left). The blocks are located on a uniform surface (see Figure 1 for a sketch of the model geometry). The effects of the substrate on the blocks are given by the static friction, F_s, and the velocity-dependent kinetic friction, F_k. This description is supported by measurement on blocks with contact area larger than some hundreds

* Corresponding author. E-Mail: urbakh@post.tau.ac.il. Telephone: +972-3-6408324. Fax: +972-3-6409293.
[†] School of Chemistry, Tel Aviv University.
[‡] Institut für Festkörperphysik, Technische Universität Darmstadt.

10.1021/nl070003a CCC: $37.00
Published on Web 02/20/2007

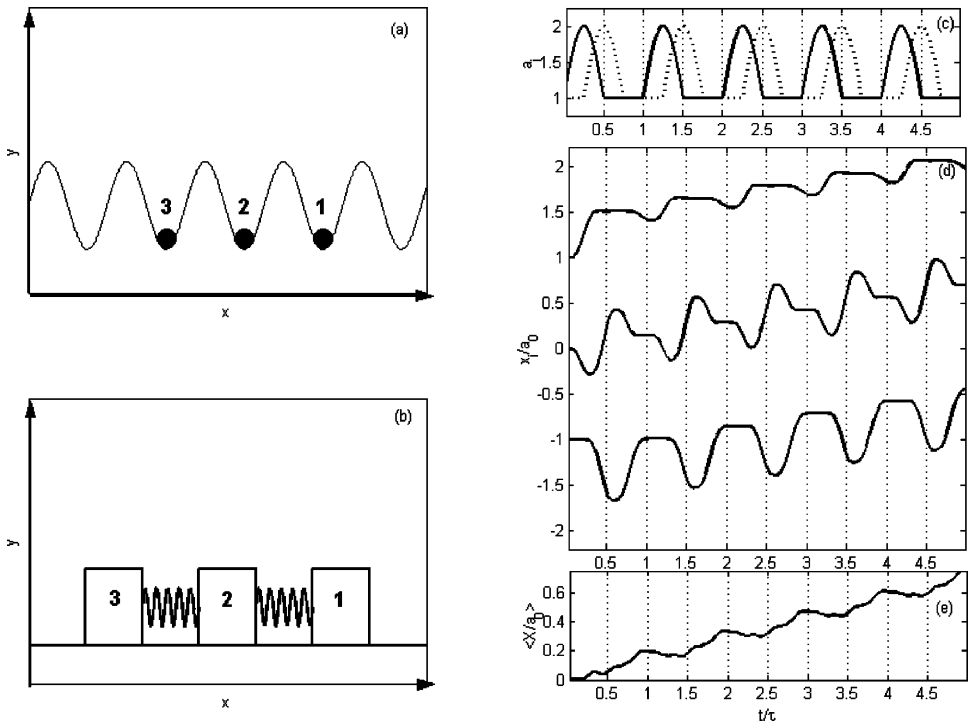

Figure 1. (a,b) Sketch of the geometry of the example engine in (a) an atomistic model[6−8] and (b) mesoscale model. (c) Free equilibrium length along 5 excitation cycles. Dotted and solid lines correspond to free equilibrium length of the front and rear springs, respectively. (d) Trajectories of the three blocks, 1−3, from top to bottom. (e) The center mass of the engine as a function of time. The parameters are: $\Delta\phi = 0.5\pi$, $\tilde{\eta} = 10$, $\tilde{F}_s = 0.25$, $\tilde{F}_k^0 = \tilde{F}_s$, $\tilde{C} = 4$.

of nanometers[9,11] which we consider here. Throughout this work, we use the following simple form of the kinetic friction

$$F_k = -F_k^0 \,\mathrm{sign}(\dot{x}_i) - \eta\,\dot{x}_i \tag{1}$$

where $\dot{x}_i$ is the velocity of the block i, sign($\dot{x}_i$) denotes the sign of $\dot{x}_i$, F_k^0 is the limiting value of the kinetic friction for zero velocity, and η is the dissipation constant. Writing the equations of motion, we have to distinguish between sticking and slippage events of a block. If it sticks, its position, x_i, does not change until the driving force, F_{dr}^i, acting on the block exceeds the static friction. Thus,

$$\dot{x}_i = 0 \text{ if } |F_{dr}^i| \le F_s \tag{2}$$

If the block slips, the equation of motion reads

$$m\ddot{x}_i = F_k + F_{dr}^i \tag{3}$$

Note that the kinetic friction force is assumed independent of the block index i. The driving forces, F_{dr}^i, arise from elastic interactions produced by the externally driven oscillations of the springs which connect the blocks. These forces can be written in the form

$$F_{dr}^i = -\frac{K}{2}\nabla_{x_i}\left[(|x_1 - x_2| - a_1(t))^2 + (|x_2 - x_3| - a_2(t))^2\right], \quad i = 1, 2, 3 \tag{4}$$

The free rest length $a_j(t)$ depends on which spring is considered, specified by the index $j = 1,2$ and on time t. The time-dependent modulation of $a_j(t)$ introduces a simple and straightforward mechanism to pump energy into the system by periodic oscillations of frequency ω. To keep the discussion simple, we will restrict ourselves to a certain choice of $a_j(t)$, resulting in a fixed spatial and temporal correlation between the lengths of different springs:

$$a_j(t) = \begin{cases} a_0 & \text{for } 2\pi n \le \omega t < \phi_j \\ a_0[1 + C\sin(\omega t - \phi_j)] & \text{for } \phi_j + 2\pi n \le \omega t < \phi_j + \pi(2n+1) \\ a_0 & \text{for } \phi_j + \pi(2n+1) \le \omega t < 2\pi(n+1) \end{cases} \tag{5}$$

Here a_0 is the rest length of the unmodulated springs, C is the amplitude of the rest length oscillation (in what follows, this parameter will be named the modulation amplitude), ω and ϕ_j are respectively the driving frequency and the phases of the spring modulation (see Figure 1c), and n is the period number. Obviously, a_0 is an intrinsic parameter of the system, and C, ω, and ϕ_j are externally adjustable. It should be noted that the phase difference, $\Delta\phi = \phi_2 - \phi_1$, rather than the phases themselves is of importance for further consideration. The model can be extended: the engine can include more than three blocks, and there is a wide range of possibilities to pump energy into the system depending on different spatially and temporally correlated changes in rest lengths.

Such oscillations can be realized experimentally, for instance, by superimposing an external frequency-dependent

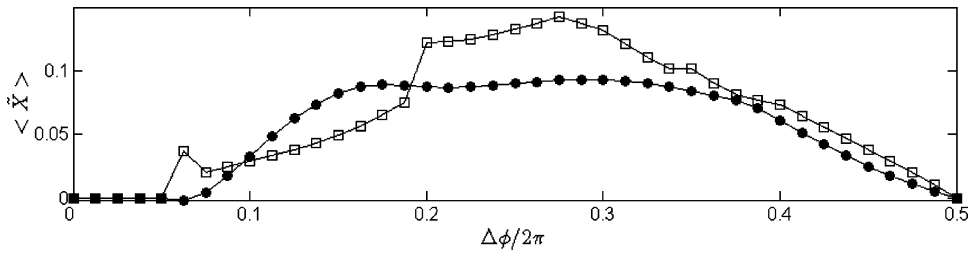

Figure 2. Dimensionless drift of the engine as a function of phase shift, $\Delta\phi$. Black circles and empty squares correspond to $F_k^0 = 0.5F_s$ and $F_k^0 = F_s$, respectively. Here $\tilde{C} = 3$, $\tilde{\eta} = 10$, $\tilde{F}_s = 0.25$.

field along the substrate whose wavelength is commensurate with dimensions of the blocks. The interaction of the varying field with the springs will provide the time dependence and phase shift needed for directed motion. Another possibility is by implementing different chromophors into the "springs" so that each spring is characterized by a different color. Exciting the system remotely can also account for the temporal and spatial patterns in the spring modulation that lead to the required motion.

To describe the motion of the engine, it is convenient to introduce dimensionless units for coordinates and time: $\tilde{x}_i = x_i/a_0$, $\tilde{t} = t/\tau$, where $\tau = 2\pi/\omega$. The dynamical behavior of the system is determined by the following dimensionless parameters: $\tilde{\eta} = \eta\tau/m$, $q = Km/\eta^2$, $\tilde{F}_s = F_s/Ka_0$, $r = F_k^0/F_s$, $\tilde{C} = C/(F_s/Ka_0)$. To characterize the motion of the engine, we discuss below the dependence of the mean displacement of the center of mass during one period of vibrations (net drift), $\langle\tilde{X}\rangle$ and the mean drift velocity $\langle V\rangle = \langle\tilde{X}\rangle/\tau$ on the system parameters; $\langle\tilde{X}\rangle = (1/(3n_{max}))\sum_{i=1}^{3}\sum_{n=1}^{n=n_{max}}[\tilde{x}_i(t = n\tau) - \tilde{x}_i(t = (n-1)\tau)]$. Most of the results presented below have been obtained for: $\Delta\phi = 0.5\pi$, $\tilde{\eta} = 10$, $\tilde{F}_s = 0.25$, $q = 1$, and $\tilde{C} = 3$.

The motion of the center of mass of the engine and its constituent blocks is shown in Figure 1d−e. Despite the fact that the average external force acting on the engine is zero, we observe a directed motion. It is important to note that at equilibrium, both the moving object and underlying surface are symmetric, and the symmetry in the system is broken dynamically through the introduction of a phase shift between the excitations of the two springs. As a result, the direction of the motion is determined dynamically and is solely given by the spring whose rest length increases first, as in the atomic scale engine.[6−8] In general, for more than two springs, the "excitation" has to propagate opposite to the desired direction of motion, starting at the block that is frontmost. Therefore, the motion can be easily controlled; in particular, the direction can be chosen independent of velocity.

To get insight into the general behavior of the engine, we performed numerical simulations of eqs 2 and 3 that describe the coupled dynamics of the blocks under externally driven oscillations of the connecting springs. First, we present in Figure 2 the dependence of the net drift, $\langle\tilde{X}\rangle$, on the phase shift, which is the crucial parameter that controls the asymmetry of the driving forces. We show $\langle\tilde{X}(\Delta\phi)\rangle$ in the interval $0 \le \Delta\phi < \pi$ only because the drift is an antisymmetric function of $\Delta\phi$ about the point, $\Delta\phi = \pi$, namely $\langle\tilde{X}(\pi + \phi)\rangle = -\langle\tilde{X}(\pi - \phi)\rangle$. Obviously the drift vanishes at $\Delta\phi = 0$ when the driving force becomes symmetric in time and space. Figure 2 shows that, for given values of C and F_s, there is a minimal value of the phase shift that is required to maintain a directed motion. For smaller values of $\Delta\phi$, the middle block remains motionless and the front and rear blocks oscillate about equilibrium positions. The value of $\Delta\phi$ defines a length of the time interval where the springs 1 and 2 work out of phase, the spring 1 contracts, and the spring 2 expands (see Figure 1c). The longer this interval is, the more efficient the engine motion is. Thus the maximal drift velocity is achieved for $\Delta\phi \simeq 0.5\pi$ when the two spring forces experienced by the middle block act in the same direction.

Figure 3 shows the net drift, $\langle\tilde{X}\rangle$, as a function of the modulation amplitude for given driving parameters (ω, $\Delta\phi$) and a given ratio between the kinetic and static friction; F_k^0/F_s. One can see that, in the case of low kinetic friction, $F_k^0 \le 0.5F_s$, five regimes of motion can be isolated, which we denote R_0−R_4. The boundaries between these regimes calculated for $F_k^0 = 0$ are labeled as $C_{th}^{(i)}$, $i = 1-4$, and are marked by dashed lines. In the first regime, R_0, where the amplitude $\tilde{C} < \tilde{C}_{th}^{(1)}$, the driving force is always lower than the static friction and the blocks remain stuck to the surface. The nature of the different dynamical regimes, R_1−R_4, can be characterized following variation of the front block velocity during one period of the excitation as shown in Figure 3b−e. In regime R_1, where $\tilde{C}_{th}^{(1)} < \tilde{C} < \tilde{C}_{th}^{(2)}$, the elongation of the front spring induces a "burst" of block motion in the positive direction, and the block remains immobile during the modulation of the rear spring (see Figure 3b). This regime can be called a one-burst regime. In the regime R_2 ($\tilde{C}_{th}^{(2)} < \tilde{C} < \tilde{C}_{th}^{(3)}$), a second burst of motion, this time in the negative direction, is caused by a contraction of the rear spring (see Figure 3c). Further increase of the modulation amplitude leads to a new, three-burst regime of motion R_3 ($\tilde{C}_{th}^{(3)} < \tilde{C} < \tilde{C}_{th}^{(4)}$), where an additional interval of negative displacement of the front block arises from a backward motion of the middle block (see Figure 3d). The operation of the engine in the regimes R_2 and R_3 is less efficient than that in the one-burst regime R_1 because of the presence of the intervals of backward motion. It should be noted that the length and duration of the bursts in regimes R_1−R_3 can be tuned with high precision by changing the modulation amplitude C. This may be useful for micromachining applications where high precision positioning requirements are of primary importance.

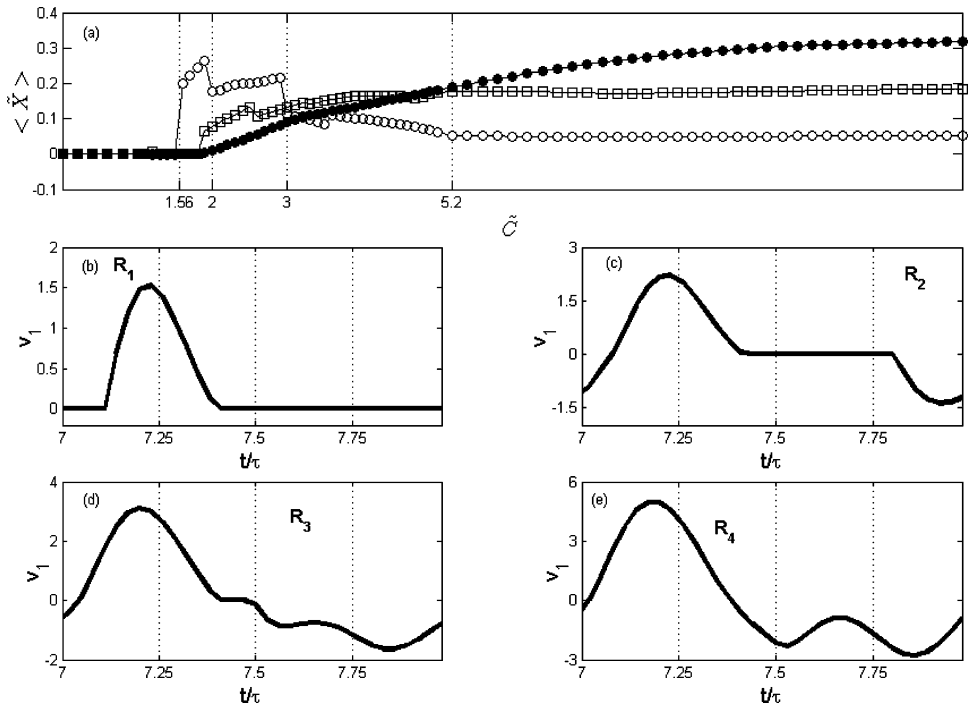

Figure 3. (a) Dimensionless drift as a function of the modulation amplitude. The results have been obtained for three values of kinetic friction, F_k^0/F_s: 0 (−○−), 0.5 (−□−), and 1 (−●−). Five regimes of motion observed at a low kinetic friction are marked as R_0, R_1, R_2, R_3, and R_4. Dotted lines show boundaries between regimes of motions found for the case $F_k = 0$. Parameter values: $\Delta\phi = 0.5\pi$, $\tilde{\eta} = 10$, $\tilde{F}_s = 0.25$. (b−e). Velocity of the front block as a function of time, for four regimes of motion: (b) R_1 ($\tilde{C} = 1.9$), (c) R_2 ($\tilde{C} = 2$), (d) R_3 ($\tilde{C} = 3$), and (e) R_4 ($\tilde{C} = 5.3$). Here $F_k^0 = 0$ and other parameters as in Figure 2.

The dynamics in regimes R_1−R_3 can be represented as a set of alternating segments of stick and slip motion of the blocks. In contrast, for high modulation amplitudes, $\tilde{C} > \tilde{C}_{th}^{(4)}$ (regime R_4), the front block constantly slides (see Figure 3e). Here the driving force acting on the front block at the turning points of its motion is always higher than the static friction, and the block never stops. In regime R_4, the static friction is of minor importance, and it is mainly the nonlinear kinetic friction that breaks the symmetry of the blocks motion and leads to a nonzero net displacement of the engine. The results presented in Figure 3a also demonstrate that, for high modulation amplitudes, the net drift of the engine becomes almost independent of the modulation amplitude. This behavior can be qualitatively understood if we describe the block motion with help of eq 3 only, justified when one can neglect the effect of static friction. Then by summing eq 3 over all blocks and going to Fourier space, we get the following expression for the drift velocity

$$\langle V \rangle = -F_k^0 \bar{s}/\eta \tag{6}$$

where $\bar{s} = (1/\tau) \int_0^\tau dt s(t)$ and $s(t) = \text{sign}[\dot{X}(t)]$ is a sign of the momentary velocity of the center of mass. Our simulations show that increasing the amplitude within regime R_4 does not change the shape of $X(t)$ and correspondingly the value of $\bar{s}$. As a result, the drift velocity reaches the plateau with increase in C. It should be noted that the regimes of motion that are similar to that described above have been found recently by considering a block motion induced by asymmetric vibrations of the underlying surface.[12,13]

An increase of kinetic friction F_k^0 washes out the boundaries between different regimes of motion, and for high kinetic friction, $F_k^0 = F_s$, the mean displacement of the center of mass, increases monotonically with the amplitude of the modulations (see Figure 3a). The engine motion can be also tuned through a variation of the frequency of oscillations. The dependence of the drift velocity on ω is determined by a competition between a time scale of external driving, $1/\omega$, and intrinsic time scales, m/η and $(m/K)^{1/2}$.

The predicted regimes of motion strongly depend on the magnitude of static and kinetic friction, which can be tuned by a chemical modification of interfaces. Figure 4 shows the dependence of the net drift $\langle \tilde{X} \rangle$ on the kinetic friction F_k^0 for four regimes of motion, R_1−R_4. For the low modulation amplitudes corresponding to the one-burst regime R_1 (the curve with gray circles in Figure 4), we found an expected reduction of the drift with increase of F_k^0. In this regime, the blocks move in the positive direction only, and under these conditions, an increase of the resistant force, $-F_k^0$ sign($\dot{x}$), reduces the overall displacement. A similar trend is observed in regime R_2 (curve −●− in Figure 4), where the blocks spend most of the time sliding in the positive direction. In contrast, a counterintuitive increase of the drift with F_k^0 has been observed for higher amplitudes (regimes R_3 and R_4, curves −□− and −○− in Figure 4). In these regimes, the front block spends most of time in backward motion, i.e., $\text{sign}(\langle \text{sign}(\dot{x}_i(t)) \rangle) \neq \text{sign}(\langle \dot{x}_i(t) \rangle)$, and an increase of the kinetic friction enhances an asymmetry of the engine motion and, as a result, intensifies a directed transport. The curve

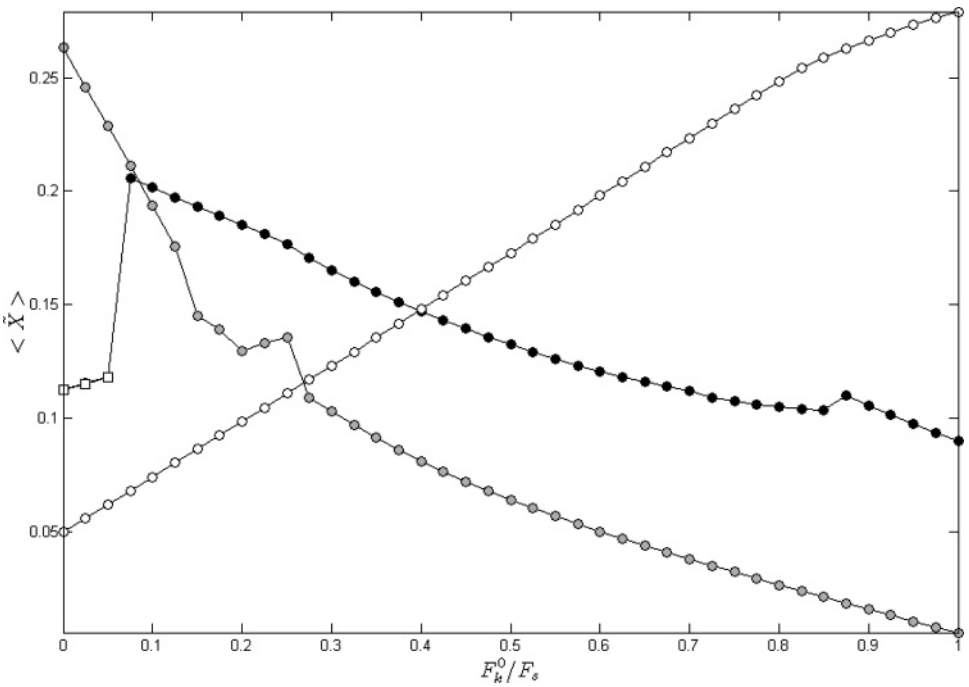

Figure 4. Dimensionless drift as a function of kinetic friction. The results have been obtained for the following values of the modulation amplitudes; $\tilde{C} = 1.9$ (curve with gray circles), $\tilde{C} = 3.0$, $F_k^0/F_s > 0.1$ (−●−), $\tilde{C} = 3.0$, $F_k^0/F_s < 0.1$ (−□−) and $\tilde{C} = 8$ (−○−), which correspond to regimes R_1, R_2, R_3, and R_4, respectively. Here $\Delta\phi = 0.5\pi$, and other parameters as in Figure 2.

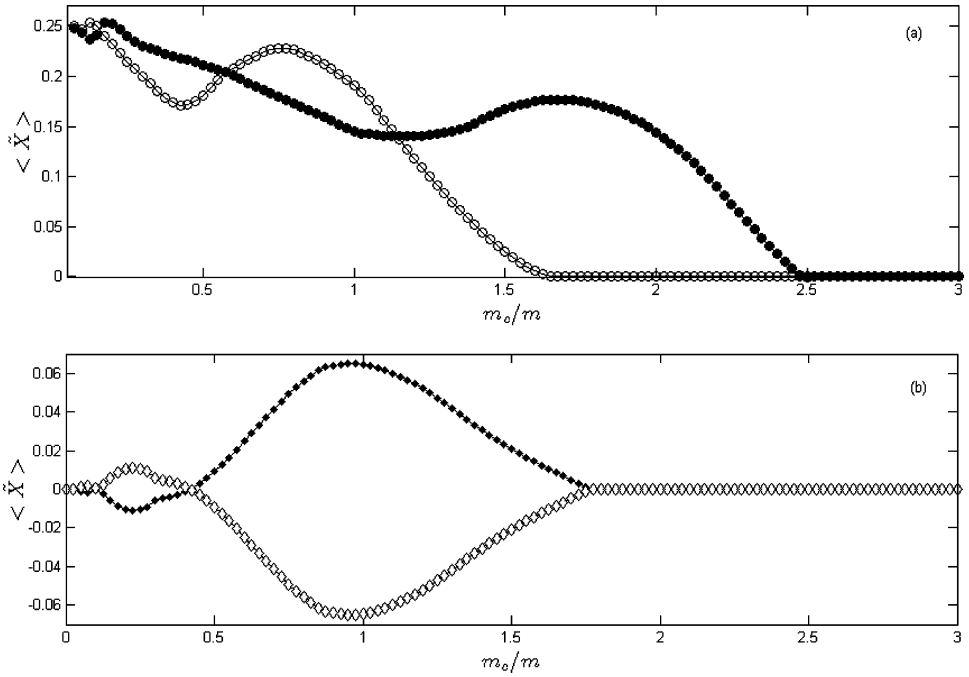

Figure 5. Dimensionless drift as a function of the mass of the cargo. Filled and empty symbols correspond to a cargo connected to the rear and front blocks, respectively. Three (a) and two (b) blocks transporting a cargo. Here $\tilde{C} = 7$, $F_k^0 = F_s$, $\Delta\phi = 0.5\pi$, and other parameters as in Figure 2.

which corresponds to the regime R_4 follows eq 6, showing a linear increase of $\langle X \rangle$ with F_k^0.

To illustrate our results, we use here the values of frictional forces measured for a microelectromechanical device (MEMS), which presents a microsize silicon block sliding on a monolayer-lubricated polycrystalline silicon surface.[14] For this system, the static and dynamic friction are dominated by adhesion (the gravitational contribution is negligible), and their values are $F_s/S = 0.95$ nN/μm^2, $F_k^0/S = 0.88$ nN/μm^2, where S is an apparent contact area, and the dissipation constant $\eta/m \approx 10^3$ s^{-1}. Then, for the blocks with area $S = 10$ μm^2 and the modulation frequency $2\pi\omega = 100$ Hz, our calculations show that directed motion can be achieved for the relative modulation amplitudes $C > 0.1$. For the above values of parameters, the mean drift velocity $V = 4.6$ μm/s is achieved for $C = 0.3$, and the corresponding burst (step)

length equals 46 nm. Varying the amplitude, C, one can get a desirable magnitude of step length ranging from a few to hundred nanometers. These estimations demonstrate that the proposed mechanism provides long-range motion with step sizes lying in the nanometer range. Hence, this approach may be useful for very high precision positioning requirements in micromachining applications.[10]

The engine is powerful enough to transport a cargo with a mass which equals about two-thirds of its own mass. To demonstrate this possibility, we attached an additional mass to the front or rear block with the spring of the same stiffness but with a *constant* (not modulated) rest length a_0. Figure 5a shows the dependence of the net drift on the mass of the pulled or pushed cargo, m_c. Performing the calculations, we assumed that static and kinetic frictional forces for the cargo are proportional to its mass, $F_{s,c} = F_s(m_c/m)$, $F^0_{k,c} = F^0_k\,(m_c/m)$. It is intriguing that the net drift does not decrease monotonically with the mass of the cargo, and there is a local maximum in the dependence of $\langle \tilde{X} \rangle$ on m_c. The reason for this is that the attachment of cargo does not only introduce an additional resistance force but also breaks the symmetry of the system. Namely, the attachment of the cargo to the rear end of the engine suppresses the backward motion and, as a result, can improve a performance of the engine. This effect explains also why pushing the cargo is more efficient than pulling, as shown in Figure 5. To stress this point, we present in Figure 5b results of calculations for the engine, which includes two blocks connected by the oscillating spring and a cargo. Without the cargo, this system is temporally and spatially symmetric, and the engine cannot perform a directed motion. In this case, only the presence of cargo destroys the symmetry and allows for a directed transport. Figure 5b shows that there is an optimal value of the mass of the cargo that leads to the most efficient motion. Obviously, attachment of the cargo to the left or to the right block of the engine results in the same absolute value of the drift velocity, but in the opposite directions of motion.

So far, our discussion has been restricted to a linear one-dimensional system. However, the above concept can be easily generalized to higher dimensionality and applied to other types of motion in a similar way as done in refs 6 and 7 for the nanoscale engine. For instance, an engine that can perform *rotational* motion may be realized if one connects three blocks via three externally driven springs forming a closed circuit. In addition, each of the blocks should be attached through a spring with a *constant* rest length to a central point, $\boldsymbol{r}_0$, which serves as a pivot. Then the force, F^i_{dr}, acting on the block i is determined by the following potential:

$$\Psi(r_i,t) = \frac{K}{2}\sum_{j\neq i}(|\boldsymbol{r}_i - \boldsymbol{r}_j| - a_{i,i\pm1}(t))^2 + \frac{K_0}{2}(\boldsymbol{r}_i - \boldsymbol{r}_0)^2 \qquad i,j = 1,2,3 \quad (7)$$

where K_0 is the stiffness of the spring connecting the block to the pivot point $\boldsymbol{r}_0$, and $a_{i,j}(t)$ are the rest lengths of the springs that join together blocks i and j. Our calculations show that, for the temporal behavior of the rest lengths given by eq 5 with the phase shift between excitation of the right and left adjacent springs equal to 0.5π, the engine makes a complete turn during three periods of excitation. Here, as in the case of the translational engine, the direction of motion is opposite to the direction of propagation of excitation. Thus the direction of rotation can be reversed by changing the order of the applied excitations.

In summary, we have investigated a new approach to build mesoscopic-size engines that move translationally or rotationally and can perform useful functions such as the pulling of a cargo. The approach is based on the transformation of internal vibrations of the moving object into directed motion by making use of nonlinear properties of friction. Characteristic of this approach is that a directed motion can be produced on a uniform substrate and thus does not require any topographical track. We have shown that direction, velocity, and length of individual bursts of the engine are determined by the frequency, amplitude, and shape of the vibrations. Realizations of the proposed concept are not limited by a particular model discussed here, and the engine can include more than three blocks; there is a wide range of possibilities to pump energy into the system depending on different spatially and temporally correlated excitations of the internal springs.

Acknowledgment. We thank Yotam Asscher for helpful discussions. J.K. and M.U. acknowledge the support by the German Research Foundation (DFG) via grant Ha 1517/26-1, 2 ("Single molecules"). M.U. acknowledges the support by the Israel Science Foundation (grant no. 1116/05).

References

(1) Balzani, V.; Credi, A.; Raymo, F. M.; Stoddart, J. F. *Angew. Chem., Int. Ed.* **2000**, *39*, 3349.
(2) Kottas, G. S.; Clarke, L. I.; Horinek, D.; Michl, J. *Chem. Rev.* **2005**, *105*, 1281.
(3) Jülicher, F.; Ajdari, A.; Prost, J. *Rev. Mod. Phys.* **1997**, *69*, 1269.
(4) Reimann, P. *Phys. Rep.* **2002**, *361*, 57.
(5) Astumian, R. D.; Hänggi, P. *Phys. Today* **2002**, *55*, 33.
(6) Porto, M.; Urbakh, M.; Klafter, J. *Phys. Rev. Lett.* **2000**, *84*, 6058.
(7) Porto, M.; Urbakh, M.; Klafter, J. *Acta Phys. Pol., B* **2000**, *32*, 295.
(8) Porto M.; Urbakh, M.; Klafter, J. *Phys. Rev. E* **2002**, *65*, 011108.
(9) Muser, M. H.; Urbakh, M.; Robbins, M. O. *Adv. Chem. Phys.* **2003**, *126*, 187.
(10) de Boer, M. P.; Luck, D. L.; Ashurst, W. R.; Maboudian, R.; Corwin, A. D.; Walraven, J. A.; Redmond, J. M. *J. Microelectromech. Syst.* **2004**, *13*, 63.
(11) Urbakh, M.; Klafter, J.; Gourdon, D.; Israelachvili, J. *Nature (London)* **2004**, *430*, 525.
(12) Buguin, A.; Brochard, F.;. de Gennes, P.-G. *Eur. Phys. J. E* **2006**, *19*, 31.
(13) Fleishman, D.; Asscher, Y.; Urbakh, M. *J. Phys.: Condens. Matter* in press.
(14) Corwin, A. D.; de Boer, M. P. *Appl. Phys. Lett.* **2004**, *84*, 2451.

NL070003A